Astronomy & Astrophysics

Simultaneous UV- and ion processing of astrophysically relevant ices

The case of $CH_3OH:N_2$ solid mixtures

F. Islam, G. A. Baratta, and M. E. Palumbo

INAF, Osservatorio Astrofisico di Catania, via Santa Sofia 78, 95123 Catania, Italy
e-mail: mepalumbo@oact.inaf.it

ABSTRACT

Context. Interstellar ices are known to be simultaneously processed by both cosmic-ray bombardment and UV photolysis. Our knowledge of the effects of energetic processing on relevant icy samples is mainly based on laboratory investigations. In the past 35 years many experiments have been performed to study these effects separately but, to the best of our knowledge, never simultaneously.

Aims. The aim of this work is to study the effects of simultaneous processing of ices by both cosmic rays and UV photons to investigate to what extent the combined effect of ion bombardment and UV photolysis influences the chemical pathways.

Methods. We carried out the simultaneous processing of $CH_3OH:N_2$ ice held at 16 K by 200 keV H^+ ions and Lyman-alpha 10.2 eV UV photons. The samples were analyzed by in situ transmission infrared spectroscopy. The un-combined processes of UV irradiation and bombardment by H^+ ions of $CH_3OH:N_2$ ice were also studied. This mixture was chosen because the effects of ion bombardment and UV photolysis on methanol and nitrogen have been extensively studied in previous investigations. This mixture enables one to investigate whether simultaneous processing (a) influences the destruction of original species; (b) influences the formation of new species; or (c) causes synergistic effects since Lyman-alpha photons have a very low efficiency in breaking the dinitrogen bond because N_2 is almost transparent at Lyman-alpha wavelengths.

Results. After processing a $CH_3OH:N_2$ sample, the intensity of the methanol bands was observed to decrease at the same rate in all cases. After ion bombardment, species such as CO_2, CO, H_2CO, CH_4, N_2O, $HNCO$, and OCN^- are formed in the ice mixture. After UV photolysis, species such as CO_2, CO, H_2CO, and CH_4 are formed, but no N-bearing species are detected. Spectra of ices processed by both UV photons and ions were compared with spectra of ices bombarded only by ions. We find that there are no differences in the band area and profile of N-bearing species for the two types of experiment at the same ion fluence; therefore, the addition of UV irradiation to ion bombardment does not affect the abundance of N-bearing species. The initial formation rate of CH_4, within the experimental uncertainties, is the same in all cases studied, while the saturation value of CH_4 is higher for UV photolysis than for ion bombardment when they act separately. In the case of simultaneous processing, when the dose (eV/16u) given by UV photons is similar to the dose given during ion bombardment, the saturation value of CH_4 reaches a value intermediate between the value obtained after UV photolysis and ion bombardment separately.

Conclusions. Our results confirm that when UV photolysis and ion bombardment act separately, their effects are very similar from a qualitative point of view, while significant quantitative difference may exist. In the case of simultaneous processing we did not detect any synergistic effect, but in some instances the behavior of newly formed species (such as CH_4) can significantly depend on the UV/ions dose ratio.

Key words. astrochemistry – molecular processes – methods: laboratory – techniques: spectroscopic – ISM: molecules

1. Introduction

The key to interstellar chemistry lies in the formation of molecules on dust grain surfaces. These dust grains are thought to be mainly silicate or carbonaceous in nature. In dense regions, such as in the interior of dense molecular clouds, dust grains provide shielding from the external galactic UV radiation field, allowing the formation of icy mantles surrounding the dust grains. The interior of molecular clouds is penetrated by cosmic rays, which are ubiquitous throughout the interstellar medium. Cosmic rays may be protons, alpha particles, nuclei of heavy atoms, electrons, and positrons (Swordy 2001). The interaction of interstellar material and cosmic rays in turn produce a number of secondary particles, such as low-energy cosmic rays, electrons, and UV photons. Thus, interstellar ices are processed simultaneously by mostly internal but also by attenuated external UV radiation as well as by fast-moving ions from the galactic cosmic radiation field. Both processes induce chemical and structural changes within the ice mantles of interstellar dust

grains (e.g., Grim et al. 1989; Jenniskens et al. 1993; Palumbo et al. 1998; Hudson et al. 2008; Palumbo et al. 2010).

The distinct processes of ion bombardment and UV irradiation on solids of astrophysical interest are well characterized (e.g., Hagen et al. 1979; Brown et al. 1982; Moore et al. 1983; Strazzulla et al. 1983a; Allamandola et al. 1988; Baratta et al. 1991; Westley et al. 1995a; Gerakines et al. 1996; Strazzulla et al. 2001; Moore et al. 2001; Leto & Baratta 2003; Öberg et al. 2009; Modica & Palumbo 2010; Garozzo et al. 2011). Some investigations on the comparison between the two processes have also been carried out. Experimental results have shown that from a qualitative point of view, ion bombardment and UV photolysis generate similar changes in interstellar ice analogs. However, quantitative differences between the two processes have been observed. Cottin et al. (2001) examined organic residues produced from $H_2O:CO:CH_3OH:NH_3$ ices after UV photolysis or proton bombardment to find that hexamethylenetetramine was present in the residue after both processes. Gerakines et al. (2000) investigated the formation of

carbonic acid (H_2CO_3) from H_2O:CO_2 ice mixtures and found that H_2CO_3 is readily formed by proton bombardment. However, in the case of UV photolysis, the penetration of UV photons into the ice limits the production of H_2CO_3. Gerakines & Moore (2001) investigated the formation of carbon suboxide (C_3O_2) in ices analogous to cometary nuclei and interstellar regions to give formation and destruction rates for C_3O_2, CO and CO_2 for both proton bombardment and UV irradiation. They found that Lyman-alpha photons are 3.5 times more efficient than 800 keV protons in synthesizing CO_2 on pristine CO per unit incident energy. Differently to Gerakines & Moore (2001), Loeffler et al. (2005) analyzed their data as a function of absorbed energy and found that the production rates (i.e., molecules formed per unit of absorbed energy) of CO_2, formed after processing of CO ice, by both 200 keV protons and Lyman-alpha photons are similar, but at saturation (i.e., when the exponential trend approaches the asymptotic value) the concentration of CO_2 is three times higher for ion bombardment.

In studies of N_2 ices, Hudson & Moore (2002) discovered that while the N_3 (azide) radical was readily formed after bombardment with 0.8 MeV protons, photolysis by far-UV did not result in the detection of N_3. However, studies by Wu et al. (2012) have shown that UV photolysis of thick (about 160 μm) solid N_2 samples does indeed produce N_3, thus it is most likely that some N_3 was produced in the experiments of Hudson & Moore, albeit in very small quantities below their detection limit. Furthermore, Kobayashi et al. (2008) irradiated gas mixtures of carbon monoxide, nitrogen, and water using UV light and particle beams of hydrogen (protons), helium, carbon, neon, and argon ions to investigate the production of amino acids. They found that when N_2 molecules were used as the nitrogen source, amino acids were not detected after photolysis with UV light, but were detected after processing with the particle beams. Kobayashi et al. ascribed this effect to the inability of UV light to dissociate either CO or N_2 molecules. From the results reported by Wu et al. (2012), assuming the density of N_2 to be about 0.83 g cm^{-3} (Roux et al. 1980), it is possible to estimate that after UV photolysis, at saturation (i.e., when the exponential trend approaches the asymptotic value) the ratio between the column densities of N_3 and initial N_2 is about 10^{-6}. Sicilia et al. (2012) reported the results of 200 keV proton bombardment of solid N_2. From their results, assuming that the band strength value for the 1657 cm^{-1} feature of N_3 is 4×10^{-17} cm/molecule (Jamieson & Kaiser 2007), it is possible to estimate that after ion bombardment with 200 keV protons at saturation the ratio between the column densities of N_3 and initial N_2 is about 10^{-4}. These experimental results show that given the same initial column density of N_2, the column density of N_3 after ion bombardment is two orders of magnitude higher than after UV photolysis.

Therefore, although ion bombardment and UV photolysis both induce similar chemical changes to interstellar ice, there are marked differences in the yields of the two processes, and as yet, it is unknown whether the two processes can affect each other.

To the best of our knowledge, only one combined experiment has been conducted with both ion bombardment and UV photolysis of interstellar-relevant ices. Baratta et al. (2002) investigated the destruction of CH_4 and CH_3OH by 30 keV He$^+$ ions and 10.2 eV Lyman-alpha photons. The effects of the two processes were found to be comparable at low doses ($\leq$20 eV/16u), such that the same number of CH_4 and CH_3OH molecules are destroyed at the same doses (see their Figs. 4 and 7). However, at high doses (>20 eV/16u), UV photolysis is less efficient in the destruction of CH_4 and CH_3OH, whereas ion bombardment

continues to induce chemical changes. This is because a residue is formed after continuous exposure to ion bombardment and UV irradiation (Moore et al. 1983; Strazzulla et al. 1983a; Strazzulla & Johnson 1991; Jenniskens et al. 1993; Ferini et al. 2004). The formation of the residue changes the optical properties of the pristine material that becomes progressively optically thick to UV radiation as processing continues. This causes the absorption coefficient to increase, therefore most UV photons are absorbed by the uppermost layers of the sample and do not penetrate the bulk of the ice, whereas the release of energy from ions into the ice remains unaffected. When a sample of CH_4 ice was first irradiated with UV up to a dose of 35 eV/16u and was then bombarded with 30 keV He$^+$ ions (from 37 eV/16u to 89 eV/16u) in a combined experiment, Baratta et al. (2002) found that the rate of CH_4 destruction by ions between doses of 40 eV/16u to 60 eV/16u increased in comparison with an experiment where the ice was bombarded by ions alone (see their Fig. 5). CH_4 molecules were found to be more efficiently destroyed by ion bombardment in an ice sample that had previously undergone UV photolysis. Therefore, it is possible that UV photolysis can enhance the process of ion bombardment.

The concept of synergy between different energetic processes in space has been considered in previous work. Westley et al. (1995a and 1995b) irradiated water-ice with Lyman-alpha photons to investigate photodesorption. They speculated that sputtering of ices by ions may be enhanced due to precursor radicals produced by UV photolysis, which may explain the difference between observations of OH near Tethys, a satellite of Saturn (Shemansky et al. 1993), and sputtering calculations (Johnson et al. 1993). In addition, they considered the possibility that an impinging cosmic ray could cause a transient temperature increase to enhance the sublimation of photolyzed ice to augment photodesorption rates.

As yet, it is unknown to what extent the combined effect of ion bombardment and UV photolysis influences the chemical pathways in icy mixtures. In this paper, we aim to investigate the effect of the occurrence of these two processes in tandem and separately on interstellar ices. To simplify this study we have considered the case of a CH_3OH:N_2 mixture. This mixture was chosen because the effects of ion bombardment and UV photolysis on methanol have been extensively studied in previous investigations (e.g., Gerakines et al. 1996; Baratta et al. 2002) and because Lyman-alpha photons have a very low efficiency in breaking the dinitrogen bond (Hudson & Moore 2002; Moore & Hudson 2003; Wu et al. 2012) because N_2 is almost transparent at Lyman-alpha wavelengths. Based on the experimental results reported by Moore & Hudson (2003) and Wu et al. (2012), we expect that the number of N-bearing species formed by UV photolysis is on the order of 10^{-4} with respect to pristine species. This amount is too low to be detected in the experimental conditions adopted in this work. On the other hand, fast ions can efficiently break N_2 molecules, giving rise to a significant number of N-bearing species. At this point, N-bearing radicals and molecules could be excited and/or broken by Lyman-alpha photons, giving rise to detectable additional (i.e., synergistic) effects. For clarity, throughout the manuscript we use the term ion bombardment to indicate ion processing, and UV photolysis or UV irradiation to indicate UV processing. The term processing is used to mean either process.

2. Experimental method

The experimental apparatus has been described in detail elsewhere (Strazzulla et al. 2001; Baratta et al. 2002; Palumbo et al. 2004). Experiments were carried out in a stainless steel
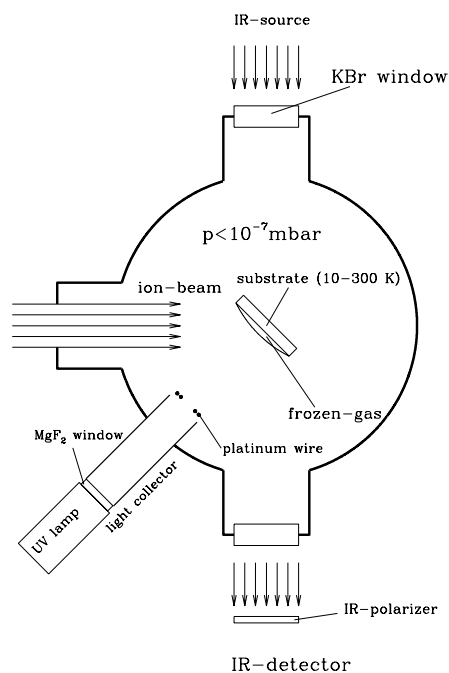
Fig. 1. Schematic view of the experimental apparatus used for in situ IR spectroscopy of frozen gases after ion bombardment and UV photolysis.

vacuum chamber shown in Fig. 1 at a base pressure of about 10^{-7} mbar. Transmission spectra were taken using a Bruker Equinox 55 FTIR spectrometer at a resolution of 1 cm^{-1} in the range 4400−400 cm^{-1} (2.27−25 μm). A silicon substrate of thickness 500 μm was cooled to 16 K by a cold-finger in thermal contact with a closed-cycle helium cryostat. Gases were admitted into the vacuum chamber through a needle valve, resulting in a background deposition of ice onto the silicon crystal. This method has the advantage that the film deposited has an uniform thickness but has the disadvantage that gas phase molecules can freeze out onto all cold surfaces inside the chamber. To avoid any deposition on the backside of the substrate, this is protected by a 2 cm long copper tube aligned with the IR beam and with the central hole with a diameter of about 4.5 mm. The thickness of the deposited ice was determined from the interference fringe curve of a reflected He-Ne laser beam following Baratta & Palumbo (1998), Fulvio et al. (2009), and Modica & Palumbo (2010).

Bombardment by 200 keV protons was performed using an electrostatic 200 kV ion implanter (Danfysik) with magnetic mass separation. The ion beams were scanned electrostatically to ensure a uniform fluence over the sample. The ion beam and the infrared beam were mutually perpendicular and formed an angle of 45 degrees with the substrate plane, thus before, during, and after bombardment, spectra could be obtained in situ without tilting the sample. The ion beam produced a spot on the target larger than the area probed by the IR beam. The current density of the ion beam must be sufficiently low to avoid macroscopic heating of the sample and typically ranged from 100 nA cm^{-2} to a few μA cm^{-2}. The ions passed through the sample without stopping, as the penetration depth of impinging ions is known to be much deeper than the sample thickness from SRIM calculations (Ziegler et al. 2008). Typically, the thickness of our samples was about 250 nm and the penetration depth of 200 keV H$^+$ in a CH$_3$OH:N$_2$ mixture was about 2 μm.

Photolysis of the sample by UV photons was carried out by means of a microwave-discharge hydrogen lamp interfaced with the vacuum chamber through a MgF$_2$ window. The discharge was produced by a continuous Opthos microwave generator operating at 2.45 GHz. The lamp was operated with a gas mixture of H$_2$ (30%) and Ar (70%) and a gas pressure P = 0.5 mbar. The lamp used in this work as well as the operating conditions were the same as used by Baratta et al. (2002) and Loeffler et al. (2005). An aluminium light collector was placed at the end of the lamp to increase the number of UV photons that reached the sample. We considered that the discharge lamps are not monochromatic and that the spectrum of the emitted radiation depends on experimental conditions, such as pressure in the discharge tube and gas mixture ratio. For example, the operating conditions adopted by Westley et al. (1995b, see their Fig. 1) produced UV photons mainly at Lyman-alpha wavelength. The operating conditions of the UV lamp adopted in this work were very similar to those used by Westley et al. (1995a,b), and we assumed that most of the photons were emitted at 121.6 nm (10.2 eV, Lyman-alpha). We developed a monitoring system of the UV flux to obtain a reliable measure of the total number of UV photons that reach the sample during photolysis (see Baratta et al. 2002). This system is described in detail in the online appendix. The flux of the lamp can be adjusted in the range 10^{12}−5 × 10^{14} cm^{-2} s^{-1}. The typical fluence of UV photons used is on the order of 10^{18} cm^{-2}.

In this study CH$_3$OH and N$_2$ were coadsorbed on a silicon substrate held at 16 K in a sandwich between layers of Ar to protect the sample from contamination by water and other background gases in the chamber. On the basis of different calibration experiments we have shown that contamination species are H$_2$O and CO$_2$, which deposit on top of the sample during processing (Loeffler et al. 2005). After further processing, CO can be formed from CO$_2$. Because of the Ar layer, these additional deposits do not affect the chemical changes induced by processing, which take place in the bulk of the sample. As shown by Loeffler et al. (2005), the deposition of background gases is significantly larger during UV photolysis than ion bombardment. In particular, after a photon fluence equal to 2.5 × 10^{18} photons cm^{-2}, the CO$_2$ column density can be as high as 2 × 10^{16} molecules cm^{-2} (Loeffler et al. 2005). As a consequence of this phenomenon, in this study we did not consider the trend of CO and CO$_2$ column density during processing.

The IR spectra may be taken by selecting the parallel (P polarization) or perpendicular (S polarization) component of the electric vector with respect to the plane of incidence using a rotatable polarizer placed in front of the detector. For each experiment, background spectra in P and S polarization were acquired before ice deposition and subtracted from all spectra with the same polarization (Baratta & Palumbo 1998; Baratta et al. 2000). P polarization spectra are presented here because the signal-to-noise ratio is higher than for S polarization.

3. Results

We deposited about 250 nm thick CH$_3$OH:N$_2$ ice sandwiched between two Ar layers on a silicon substrate held at 16 K. The samples were processed by 200 keV H$^+$ and 10.2 eV Lyman-alpha photons separately and in tandem. For the simultaneous processing, two different experiments were performed with a different ratio between UV and ion fluence. A list of the experiments is given in Table 1.

Figure 2 shows the spectra, in optical depth scale, relative to the CH$_3$OH:N$_2$ mixture as deposited (panel a), after ion

Table 1. Details of experiments.

Processing	Max UV fluence (photons cm^{-2})	Max UV dose[a] (eV/16u)	Max ion fluence (ions cm^{-2})	Max ion dose[a] (eV/16u)
Ion bombardment	–	–	1.36×10^{15}	36
UV photolysis	3.25×10^{18}	55	–	–
Simultaneous	1.76×10^{18}	34	1.29×10^{14}	3
Simultaneous	1.76×10^{18}	33	8.54×10^{14}	23

Notes. [a] Here the dose is the energy released to the target molecules in eV per small molecule (16u), where u is the unified atomic mass unit (see text).
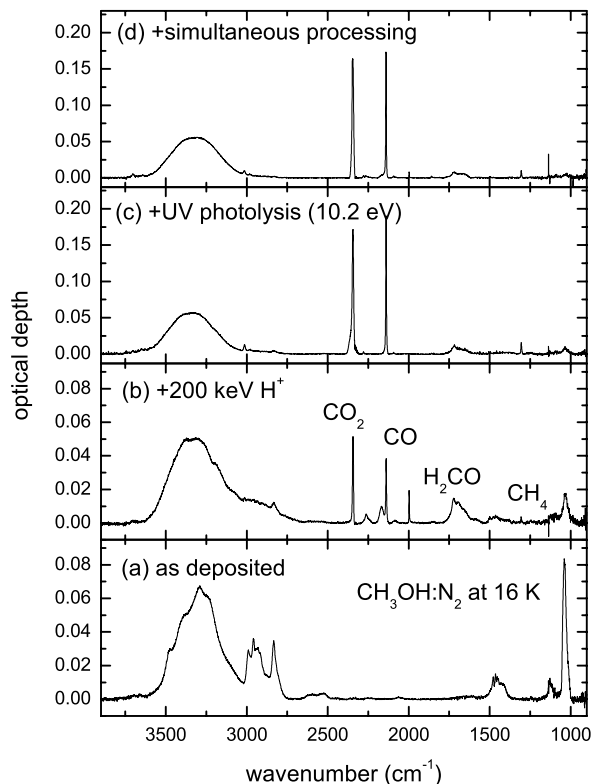

Fig. 2. IR transmittance spectra in optical-depth scale (P polarization) of CH$_3$OH:N$_2$ ice (about 250 nm thick) deposited at 16 K as deposited; after bombardment with 3.91×10^{14} 200 keV H$^+$ cm^{-2} (dose = 10 eV/16u); after photolysis with 2.42×10^{18} photons cm^{-2} (dose = 41 eV/16u); after simultaneous processing with 1.29×10^{14} 200 keV H$^+$ cm^{-2} and 1.76×10^{18} photons cm^{-2} (total dose = 37 eV/16u).

Fig. 3. Normalized methanol column density as a function of dose for the UV photolysis, ion bombardment, and simultaneous processing.

bombardment (panel b), after UV photolysis (panel c), and after simultaneous processing (panel d). Changes in the intensity of the methanol bands at 1039 cm^{-1} (C-O stretch), 1129 cm^{-1} (-CH$_3$ rock), 1460 cm^{-1} (C-H deformation and O-H bend), 2830 cm^{-1} (symmetric C-H stretch), 2961 cm^{-1} (asymmetric C-H stretch), and 3260 cm^{-1} (O-H stretch) indicate that destruction of methanol occurs after processing.

To compare the effects that are induced by fast ions and UV photons, the irradiation dose was derived (energy released onto the target molecules, i.e., eV molecule^{-1}). As suggested by Strazzulla & Johnson (1991), the dose given in units of eV per small molecule (16u) is a convenient way to characterize chemical changes and to compare the results obtained after processing of different samples. The energy released into the sample by impinging ions or photons (dose) is then given in eV/16u, where u is the unified atomic mass unit defined as 1/12 of the mass of an isolated atom of carbon-12. For the ion bombardment,
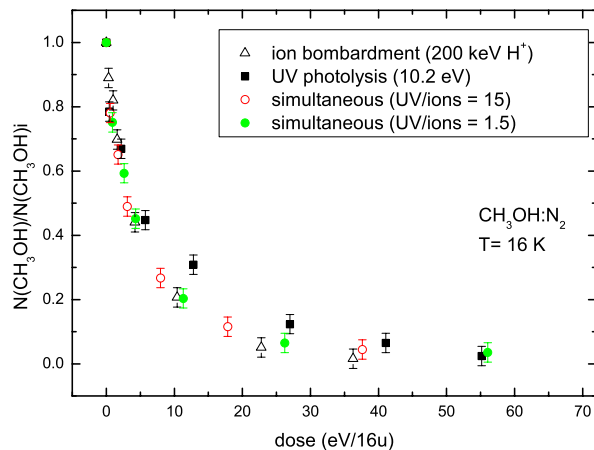
the dose (eV/16u) was obtained from the ion fluence values (ions cm^{-2}) measured during the experiment and the stopping power S (eV cm^2 molecule^{-1}) calculated using the SRIM code (Ziegler et al. 2008). For the UV photolysis, the dose (eV/16u) was obtained from the UV fluence (photons cm^{-2}) measured during the experiment and the absorption cross-section of Lyman-alpha photons in CH$_3$OH ($\sigma_a = 6.37 \times 10^{-18}$ cm^2) given by Baratta et al. (2002) assuming that the absorption coefficient of Lyman-alpha photons in N$_2$ is negligible. Two experiments with simultaneous processing were performed. In the first experiment, the dose given by UV photons was on average 15 times higher than the dose given by 200 keV protons. In the second experiment the dose ratio was about 1.5.

After processing the pristine CH$_3$OH:N$_2$ ice, the IR spectra showed a reduction in methanol abundance. Figure 3 shows the column density of methanol normalized to the initial methanol column density as a function of dose for the UV photolysis, ion bombardment, and simultaneous processing. The column density of methanol was derived from the band at about 1039 cm^{-1} after the transmittance spectrum was converted to optical depth scale and using the band strength value $A = 1.3 \times 10^{-17}$ cm molecule^{-1} (Palumbo et al. 1999). As discussed by Baratta et al. (2002), at low doses the trend of methanol column density is very similar in all cases, while at high doses the destruction of methanol is slightly slower in the case of UV photolysis. This effect can be ascribed to the change of the optical properties of the sample during processing. The optical constants of the sample change in all cases due to energetic processing. It is well known that C-bearing species evolve toward a polymer-like material and eventually to a refractory residue (Moore et al. 1983; Strazzulla et al. 1983a; Strazzulla & Johnson 1991; Jenniskens et al. 1993; Ferini et al. 2004). The
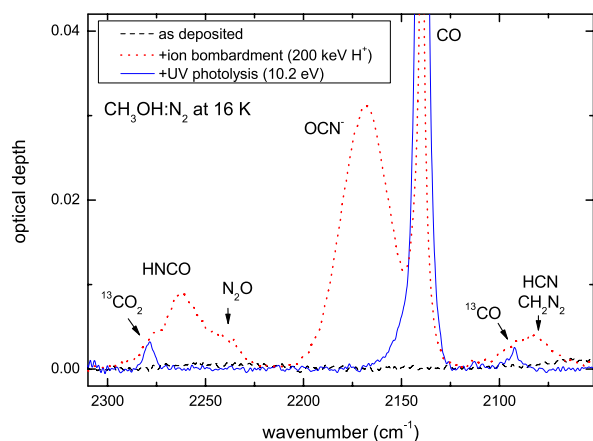
Fig. 4. IR transmittance spectra in optical-depth scale (P polarization) of $CH_3OH:N_2$ ice (about 250 nm thick) deposited at 16 K before processing (dashed line), after bombardment with 1.36×10^{15} 200 keV H^+ cm^{-2} (dose = 36 eV/16u; dotted line), and after photolysis with 2.42×10^{18} photons cm^{-2} (dose = 41 eV/16u; solid line). HNCO, N_2O, OCN^-, HCN, and CH_2N_2 are not detected after UV irradiation.

energy released by ions is independent of the optical constants of the sample, and at high doses impinging ions continue to release energy through the whole thickness of the sample and thus an additional modification of the sample occurs; on the other hand, the absorption coefficient of the refractory residue is higher than that of the pristine ice, and UV photons cause minor additional modifications to the deeper layers of the sample as photolysis proceeds.

The experimental data were fitted by the exponential curve

$$y = e^{-\sigma D}, \tag{1}$$

where y is the normalized column density of methanol, σ is the cross section (in 16u/eV), and D is the dose in (eV/16u). We obtained an average destruction cross-section for methanol equal to 0.19 ± 0.03 16u/eV.

After ion bombardment, newly formed species such as CO_2 (2343 cm^{-1}), CO (2138 cm^{-1}), H_2CO (1728 cm^{-1}), CH_4 (1305 cm^{-1}), N_2O (2235 cm^{-1}), HNCO (2263 cm^{-1}), and OCN^- (2168 cm^{-1}) were detected in the ice mixture (Figs. 2 and 4). There is also a broad feature at about 2080 cm^{-1} that may be attributed to some combination of HCN and CH_2N_2 (Grim & Greenberg 1987; Sandford & Allamandola 1990; Elsila et al. 1997; Demyk et al. 1998; Novozamsky et al. 2001; Hudson et al. 2001; Moore & Hudson 2003). The formation of N-bearing species indicates that the N ≡ N bond has been broken by ions. A weak feature is present at about 2327 cm^{-1}, which is assigned to N_2. In fact, N_2 has no infrared active bands because it is a homonuclear molecule; but in the solid phase the symmetry is broken and a weak band appears because of the interaction with neighboring molecules (Sandford et al. 2001).

Although methanol is destroyed for the UV photolysis, only species such as CO_2, CO, H_2CO, and CH_4 are detected while the amount of any N-bearing species is below the detection limit (Figs. 2 and 4). As expected from the work of Hudson & Moore (2002), N_3 was not detected. Wu et al. (2012) have shown that for very thick layers of N_2 ice (160 μm), N_3 can be detected after UV photolysis. Given that the ratio of N_3 to N_2 formed by UV photolysis is approximately 10^{-6} (Wu et al. 2012), for our sample thickness of 250 nm, where N_2 constitutes about half of the ice, we predict that any N_3 band at 1657 cm^{-1}, assuming that the width is 3 cm^{-1}, will have a peak optical depth of about
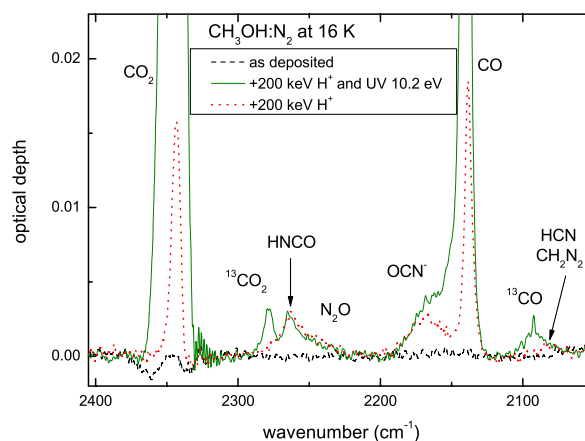
Fig. 5. IR transmittance spectra in optical depth-scale (P polarization) of $CH_3OH:N_2$ ice (about 250 nm thick) deposited at 16 K before (dashed line), after bombardment with 1.58×10^{14} 200 keV H^+ cm^{-2} alone (dose = 4 eV/16u; dotted line) and after simultaneous processing with 1.29×10^{14} 200 keV H^+ cm^{-2} and 1.76×10^{18} photons cm^{-2} (total dose = 37 eV/16u; solid line). N-bearing species such as HNCO, N_2O, OCN^-, HCN, and CH_2N_2 are formed.

5×10^{-6}, which is well below the level of noise in our spectra ($\tau_{noise} \sim 10^{-4}$).

In comparing panels (b) and (c) in Fig. 2, it is apparent that relatively more CO and CO_2 is produced by UV photolysis than by ion bombardment. As discussed in Sect. 2, the amount of CO and CO_2 detected by IR spectroscopy is affected by the problem that UV photons cause desorption of H_2O and CO_2 from the walls of the vacuum chamber, followed by deposition of these species on top of the Ar layer of the sample. CO is then formed by UV photolysis of CO_2 molecules. This effect is negligible for the ion bombardment experiments because the ion beam is well focused on the sample and does not hit the walls of the vacuum chamber.

An IR spectrum taken after the simultaneous processing of $CH_3OH:N_2$ ice by both H^+ ions and UV photons is shown in Figs. 2 and 5. The simultaneous processes destroy methanol and cause the formation of species such as CO_2, CO, H_2CO, CH_4, N_2O, HNCO, OCN^-, and CH_2N_2. As expected, ion bombardment efficiently breaks up the N_2 molecule to produce N-bearing species. Also, comparatively large abundances of CO and CO_2 are produced due to UV photolysis.

As discussed above, N-bearing species are not expected to be detected after UV photolysis in our experimental conditions. Therefore a comparison was made between the spectra of samples processed by ions and UV, and spectra relative to a sample bombarded only by ions at the same ion fluence to study the formation of N-bearing species (namely HNCO and OCN^-) after simultaneous processing. This spectral region also contains strong $^{13}CO_2$ (2278 cm^{-1}) and CO (2138 cm^{-1}) bands that overlap with the HNCO (2263 cm^{-1}) and OCN^- (2168 cm^{-1}) bands, respectively. To better compare the effects of the different processing, the spectrum relative to the UV photolyzed sample was subtracted from the spectrum of the ion- and UV processed sample. This corrected spectrum for simultaneous ion bombardment and UV irradiation was compared with the spectrum for the ions-only experiment at the same ion fluence, as shown in Fig. 6. Clearly, the spectra in Fig. 6 exhibit very similar band profiles and intensities, indicating that the abundances of HNCO and OCN^- are not affected by UV photolysis when simultaneous energetic processing takes place.
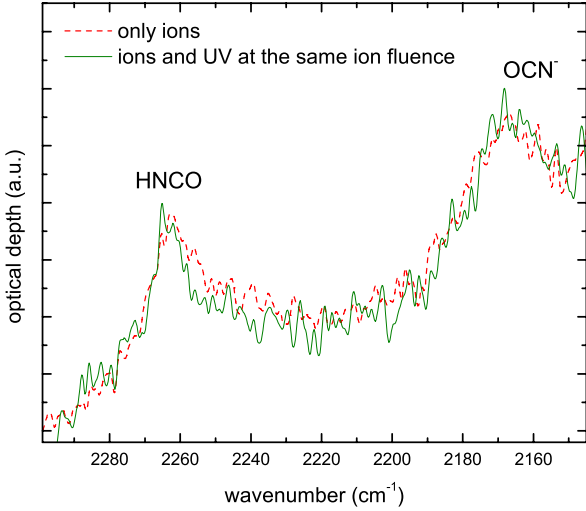
Fig. 6. IR transmittance spectra in optical-depth scale (P polarization) of CH$_3$OH:N$_2$ ice (about 250 nm thick) deposited at 16 K after bombardment with 1.58×10^{14} 200 keV H$^+$ cm^{-2} (dose = 4 eV/16u; dashed line) and after processing by a combination of 1.29×10^{14} 200 keV H$^+$ cm^{-2} and 1.76×10^{18} photons cm^{-2} (total dose = 37 eV/16u) with the band profile contribution from CO and ^{13}CO$_2$ produced by UV photolysis removed (solid line). The band profiles and intensities of HNCO and OCN$^-$ are similar for both spectra.

Figure 7 shows the column density of CH$_4$ as a function of dose. The column density of CH$_4$ was derived from the spectra in optical-depth scale from the band at about 1310 cm^{-1} using the band strength value $A = 6.4 \times 10^{-18}$ cm molecule^{-1} (Mulas et al. 1998). For each experiment the CH$_4$ column density was normalized to the initial CH$_3$OH column density. At the beginning of processing, the CH$_4$ column density increased rapidly; it reached the highest value when the dose increased and after further processing it started to decrease. The figure shows that at the beginning (i.e., at low dose) the formation rate of CH$_4$ is the same regardless of the processing. On the other hand, the highest CH$_4$ column density value reached after UV photolysis was about three times higher than the maximum amount reached after ion bombardment. As discussed above, for CH$_3$OH destruction, this is caused by the change of the optical constants of the sample after processing. Furthermore, similarly to the discussion by Loeffler et al. (2005), in the case of ^{13}CO$_2$ formation after processing of pure ^{13}CO, this could be caused by the different ratio between the formation and destruction cross-section of CH$_4$ by 200 keV protons and Lyman-alpha photons. For the simultaneous processing, the highest CH$_4$ column density depends on the ratio between the UV and ion dose during the experiments. When the UV dose prevails (average dose ratio = 15), the highest CH$_4$ column density is similar to the value reached after UV photolysis whereas when UV and ion doses are similar (dose ratio = 1.5), the highest CH$_4$ column density is an intermediate value between the value obtained after UV photolysis and the value obtained after ion bombardment.

The experimental data (from dose = 0 to the dose value at which the highest CH$_4$ column density is reached) were fitted with an exponential curve

$$y = y_\infty (1 - e^{-\sigma D}), \qquad (2)$$

where y_∞ is the asymptotic value, σ is the cross section (in 16u/eV) and D is the dose (in eV/16u). The formation rate (R in 16u/eV) was obtained from the equation

$$R = y_\infty \times \sigma. \qquad (3)$$

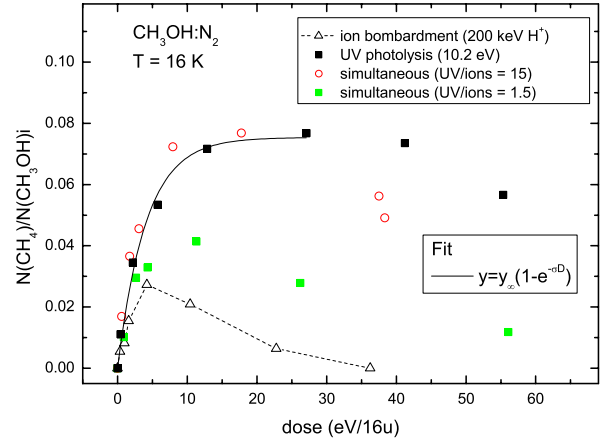**Fig. 7.** Column density of CH$_4$ formed after processing of CH$_3$OH:N$_2$ mixtures at 16 K. The CH$_4$ column density is normalized to the initial CH$_3$OH column density for each sample. The solid line is the fit of the experimental data relative to UV photolysis by an exponential curve. The dashed line connecting data points relative to ion bombardment has been drawn to guide the eye.

The parameters resulting from the fit and R values are listed in Table 2.

4. Discussion

Interstellar ices are known to be simultaneously processed by both cosmic-ray bombardment and UV photolysis. It has been estimated that in dense molecular clouds the flux of cosmic ions is 1 cm^{-2} s^{-1} in the approximation of effective monoenergetic 1-MeV protons (Mennella et al. 2003). This flux must be regarded as an effective quantity. It represents the flux of 1 MeV protons, which gives rise to the ionization rate produced by the cosmic-ray spectrum if hydrogen were the only source for ionization. As discussed by Prasad & Tarafdar (1983), an internal UV flux, $F(UV)$, is present in dense molecular clouds due to the cosmic-ray-induced fluorescence of molecular hydrogen. Depending on the assumed cosmic-ray spectrum at low energy, Shen et al. (2004) obtained $F(UV) = 2 \times 10^3 - 3 \times 10^4$ photons cm^{-2} s^{-1}.

In our laboratory investigations we used 200 keV protons; based on experimental results, the best assumption we can make is that the chemical effects depend on the total dose (eV molecule^{-1}) deposited onto the sample, therefore these effects scale with the stopping power of impinging ions (e.g., Palumbo 2006; Sicilia et al. 2012).

Recently, Shen et al. (2004) estimated the energy deposition onto water-ice grain mantles by cosmic rays and by UV photons in dense molecular clouds. They found that depending on the assumed cosmic-ray spectrum at low energy, after 10^7 years the dose deposited by UV photons varies in the range $100-10$ eV/molecule and the dose deposited by cosmic rays varies in the range $10-1$ eV/molecule. Based on these results, the energy input by UV photons is about an order of magnitude higher than the energy input by cosmic-ray particles. This means that our experimental results are fully representative of the dose range deposited by UV photons and cosmic rays on icy grain mantles in dense molecular clouds.

Moore (1999) showed that in diffuse regions UV photons deposit more energy in the icy mantles than 1 MeV protons. In particular, after 10^7 years the dose deposited by UV photons is on the order of 10^6 eV/molecule and the dose deposited

Table 2. Best-fit parameters for the formation of CH_4 after energetic processing of a $CH_3OH:N_2$ mixture at 16 K.

Processing	Asymptotic value $N(CH_4)/N(CH_3OH)i$	σ^a (16u/eV)	R^b (16u/eV)
Ion bombardment	0.037 ± 0.007	0.3 ± 0.1	0.012 ± 0.007
UV photolysis	0.075 ± 0.003	0.24 ± 0.03	0.018 ± 0.003
Simultaneous (dose ratio = 15)	0.077 ± 0.003	0.34 ± 0.04	0.026 ± 0.005
Simultaneous (dose ratio = 1.5)	0.042 ± 0.003	0.39 ± 0.06	0.016 ± 0.004

Notes. [a] Cross section σ given by Eq. (2). [b] Formation rate R given by Eq. (3).

by low-energy cosmic rays is on the order of 30 eV/molecule. This result is obtained assuming that the flux of 1 MeV protons is about 10 cm^{-2} s^{-1} (Strazzulla & Johnson 1991; Indriolo & McCall 2012) and the flux of UV photons is about 9.6×10^7 photons cm^{-2} s^{-1} (Jenniskens et al. 1993). As suggested by Westley et al. (1995a), in diffuse regions ice mantles are not observed because the photon induced desorption rate is higher than the gas adsorption rate, implying rapid removal of a pre-existing ice mantle.

In a recent work, Pedersen & Gómez De Castro (2011) have modeled the disk of a young stellar object assuming that the UV radiation field of a T Tauri star at 500 AU from the central object is 2.9×10^{10} photons cm^{-2} s^{-1}. Strazzulla et al. (1983b) have estimated that the flux of 1 MeV protons in a T Tauri star is 2×10^{10} cm^{-2} s^{-1} at 1 AU. Assuming that the flux decreases with distance as d^{-2}, at 500 AU the value is 8×10^4 cm^{-2} s^{-1}. Using the same hypothesis as Moore (1999), UV photons deposit more energy in the icy mantles than 1 MeV protons also in circumstellar regions. However, when planetesimals form, UV photons are absorbed in the external layers (on the order of 10^2 nm) while energetic ions can penetrate the bodies and release their energy in deeper layers.

As another example, it has been shown that cosmic rays can alter the outer few meters of a cometary nucleus. On the other hand, the penetration depth of UV photons is lower than that of ions and their contribution can be neglected (e.g., Strazzulla & Johnson 1991; Modica et al. 2012). It has been estimated that near the surface the dose deposited by cosmic rays after 10^9 years is as high as hundreds of eV/16u; therefore, volatile species eventually formed by cosmic-ray bombardment would be quickly destroyed by the same mechanism. At deeper layers from the surface, the absorbed dose decreases and doses as low as a few eV/16u, still able to produce noticeable chemical effects, are accumulated at depths on the order of tens of meters.

We have considered a $CH_3OH:N_2$ mixture. It might be argued that observations indicate that water ice is the most abundant solid-phase species in cometary and interstellar ices. Accordingly, the study of water-rich ice mixtures should be considered. However, in our experiments the initial thickness of the ice samples was chosen as a compromise between a sample thick enough to obtain infrared spectra with a good signal-to-noise ratio and thin enough to be uniformly processed by ions and UV photons. If we add water to the mixture (without increasing the thickness of the sample), we reduce the amount of CH_3OH and N_2, reducing in turn the amount of N-bearing species formed after processing. This reduction would make the detection of these species even more difficult. On the other hand, recent laboratory experiments (e.g., Fuchs et al. 2009) have shown that CH_3OH molecules efficiently form after hydrogenation of CO molecules in CO-rich and water-poor ices. Therefore it is reasonable to assume that CH_3OH-rich and water-poor ice mantles may exist along the line of sight of dense molecular clouds

(e.g., Skinner et al. 1992; Palumbo & Strazzulla 1992; Cuppen et al. 2011).

Most of our knowledge on the effects of UV photons and low-energy ions on astrophysically relevant ices is based on laboratory simulations. In the past 35 years, several experiments have been performed in different laboratories to study these effects separately but, to the best of our knowledge, never simultaneously. Here we have presented an experimental study of the effects of simultaneous processing on a $CH_3OH:N_2$ mixture at 16 K. Our results confirm that when UV photolysis and ion bombardment act separately, from a qualitative point of view their effects are very similar but significant quantitative differences may exist. We did not detect any synergistic effect after simultaneous processing, but from a quantitative point of view the behavior of newly formed molecules (such as CH_4, see Fig. 7) can in some instances significantly depend on the UV/ions dose ratio. Hence the effects of simultaneous processing on other astrophysically relevant mixtures should be experimentally investigated to better understand the chemical evolution of solid phase molecules in space.

Appendix A: Monitoring system of the UV flux during irradiation

We developed a monitoring system of the UV flux to obtain a reliable measure of the total number of UV photons that reach the sample during photolysis (see Baratta et al. 2002). This was obtained by measuring the current produced by the photoelectric effect on a platinum wire placed at the end of the aluminium light collector. The integrated current C (μC) measured by the wire detector is proportional to the photon fluence Φ_{ph} (cm^{-2}), which is the total UV photon number per square centimeter that reaches the sample. In particular,

$$\Phi_{ph} = M_{cal} \cdot C, \tag{A.1}$$

where M_{cal} is the calibration constant. The calibration constant of the wire was determined by measuring the O_2 to O_3 conversion rate in a UV photolyzed O_2 ice film (see Gerakines et al. 1996, 2000; Baratta et al. 2002). Following Gerakines et al. (2000), we assumed a conversion efficiency of O_2 to O_3 equal to the quantum yield Y measured for the gas phase by Groth (1937), corresponding to 1.92 ozone molecules produced for each absorbed UV photon in the O_2 film. The ozone production was monitored through the 1040 cm^{-1} band by using a band strength value of 1.4×10^{-17} cm molecule^{-1} (Smith et al. 1985). If we consider an O_2 film of thickness t (cm), the column density
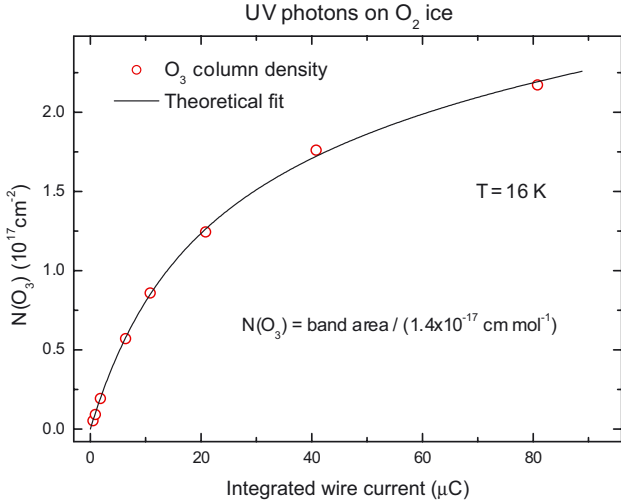
Fig. A.1. O_3 column density at different photon fluences as a function of integrated current detected. A theoretical fit obtained by a nonlinear least-squares routine is used to provide n^∞, α, and s as best-fit parameters.

of O_3 molecules $N(\Phi_{ph}, t)$ (cm^{-2}) formed in the film after a photon fluence Φ_{ph} (cm^{-2}) can be computed through the equation

$$N(\Phi_{ph}, t) = n^\infty \int_0^t \left(1 - e^{-\sigma \Phi e^{-\alpha x}}\right) dx \quad (A.2)$$

where n^∞ is the O_3 number density at saturation (cm^{-3}), that is, when the number of O_3 molecules formed (O_2 to O_3) is equal to the number of O_3 molecules destroyed (O_3 to O_2); α is the absorption coefficient (cm^{-1}) at Lyman-alpha of the irradiated O_2 film and σ is the cross section of the process (cm^2). Equation (A.2) takes into account the exponential decay of the UV flux with the depth x (cm) within the film. By substituting Eq. (A.1) in Eq. (A.2), the column density can be written versus the integrated current,

$$N(C, t) = n^\infty \int_0^t \left(1 - e^{-sCe^{-\alpha x}}\right) dx, \quad (A.3)$$

where $s = \sigma \cdot M_{cal}$. Equation (A.3) can be used to fit the experimental data acquired during the calibration experiment. In Fig. A.1, the O_3 column density at different photon fluences versus the integrated current is reported together with the theoretical fit obtained by a nonlinear least-squares routine that provides n^∞, α, and s as best-fit parameters. The film thickness t in Eq. (A.3) was computed by using the laser interference method.

The quantum yield Y can be related to the initial O_3 formation rate when t approaches ∞ in Eq. (A.3). Indeed, in this case, all the UV photons are absorbed by an oxygen molecule since the amount of O_3 molecules is negligible at very low fluence.

It follows that

$$\lim_{C \to 0} \frac{dN(C, \infty)}{dC} = Y \frac{d\Phi_{ph}}{dC}. \quad (A.4)$$

From Eq. (A.3):

$$\lim_{C \to 0} \frac{dN(C, \infty)}{dC} = \frac{n^\infty \cdot s}{\alpha}. \quad (A.5)$$

From Eq. (A.1):

$$\frac{d\Phi_{ph}}{dC} = M_{cal}, \quad (A.6)$$

and finally,

$$M_{cal} = \frac{n^\infty \cdot s \cdot \beta}{\alpha \cdot Y}, \quad (A.7)$$

where the β factor (=0.93) takes into account a 10% UV photon loss by reflection and diffusion and the increased optical path due to the IR beam oblique incidence. The calibration constant depends on the geometry of the experimental set-up, that is, the relative positions of the microwave cavity of the lamp, the aluminium light collector, and the target. The geometry can be slightly different each time the UV lamp is mounted on the vacuum chamber; for this reason we performed the calibration every time the UV lamp was mounted. We found that the calibration constant was roughly the same before and after each UV photolysis section, and it varied in the range between 4×10^{15} and 6×10^{15} cm$^{-2} \mu$C^{-1} among different sections. The flux of the lamp can be adjusted in the range 10^{12}–5×10^{14} cm^{-2} s^{-1}.

References

Allamandola, L. J., Sandford, S. A., & Valero, G. J. 1988, Icarus, 76, 225
Baratta, G. A., & Palumbo, M. E. 1998, J. Opt. Soc. Am. A, 15, 3076
Baratta, G. A., Spinella, F., Leto, G., Strazzulla, G., & Foti, G. 1991, A&A, 252, 421
Baratta, G. A., Palumbo, M. E., & Strazzulla, G. 2000, A&A, 357, 1045
Baratta, G. A., Leto, G., & Palumbo, M. E. 2002, A&A, 384, 343
Brown, W. L., Lanzerotti, L. J., & Johnson, R. E. 1982, Science, 218, 525
Cottin, H., Szopa, C., & Moore, M. H. 2001, ApJ, 561, L139
Cuppen, H. M., Penteado, E. M., Isokoski, K., van der Marel, N., & Linnartz, H. 2011, MNRAS, 417, 2809
Demyk, K., Dartois, E., d'Hendecourt, L., et al. 1998, A&A, 339, 553
Elsila, J., Allamandola, L. J., & Sandford, S. A. 1997, ApJ, 479, 818
Ferini, G., Baratta, G. A., & Palumbo, M. E. 2004, A&A, 414, 757
Fuchs, G., W., Cuppen, H. M., Ioppolo, S., et al. 2009, A&A, 505, 629
Fulvio, D., Sivaraman, B., Baratta, G. A., Palumbo, M. E., & Mason, N. J. 2009, Spectrochimica Acta Part A: Molecular Spectroscopy, 72, 1007
Garozzo, M., La Rosa, L., Kanuchova, Z., et al. 2011, A&A, 528, A118
Gerakines, P. A., & Moore, M. H. 2001, Icarus, 154, 372
Gerakines, P. A., Schutte, W. A., & Ehrenfreund, P. 1996, A&A, 312, 289
Gerakines, P. A., Moore, M. H., & Hudson, R. L. 2000, A&A, 357, 793
Grim, R. J. A., & Greenberg, J. M. 1987, ApJ, 321, L91
Grim, R. J. A., Greenberg, J. M., de Groot, M. S., et al. 1989, A&AS, 78, 161
Groth, W. 1937, Z. Phys. Chem., 37, 307
Hagen, W., Allamandola, L. J., & Greenberg, J. M. 1979, Ap&SS, 65, 215
Hudson, R. L., & Moore, M. H. 2002, ApJ, 568, 1095
Hudson, R. L., Moore, M. H., & Gerakines, P. A. 2001, ApJ, 550, 1140
Hudson, R. L., Palumbo, M. E., Strazzulla, G., et al. 2008, in The Solar System Beyond Neptune, 507
Indriolo, N., & McCall, B. J. 2012, ApJ, 745, 91
Jamieson, C. S., & Kaiser, R. I. 2007, Chem. Phys. Lett., 440, 98
Jenniskens, P., Baratta, G. A., Kouchi, A., et al. 1993, A&A, 273, 583
Johnson, R. E., Grosjean, D. E., Jurac, S., & Baragiola, R. A. 1993, EOS, 74, 572
Kobayashi, K., Ogawa, T., Tonishi, H., et al. 2008, Electron. Commun. Jap., 91, 293
Leto, G., & Baratta, G. A. 2003, A&A, 397, 7
Loeffler, M. J., Baratta, G. A., Palumbo, M. E., Strazzulla, G., & Baragiola, R. A. 2005, A&A, 435, 587
Mennella, V., Baratta, G. A, Esposito, A., Ferini, G., & Pendleton, Y. J. 2003, ApJ, 587, 727
Modica, P., & Palumbo, M. E. 2010, A&A, 519, A22
Modica, P., Palumbo, M. E. & Strazzulla, G. 2012, Planet Space Science, 73, 425
Moore, M. H. 1999, in Solid Interstellar Matter: the ISO Revolution, eds. L. d'Hendecourt, C. Joblin, & A. Jones (New York: Springer-Verlag,), 199
Moore, M. H., & Hudson, R. L. 2003, Icarus, 161, 486
Moore, M. H., Donn, B., Khanna, R., & A'Hearn, M. F. 1983, Icarus, 54, 388
Moore, M. H., Hudson, R. L., & Gerakines, P. A. 2001, Spectrochimica Acta, 57, 843
Mulas, G., Baratta, G. A., Palumbo, M. E., & Strazzulla, G. 1998, A&A, 333, 1025
Novozamsky, J. H., Schutte, W. A., & Keane J. V. 2001, A&A, 379, 588

Öberg, K. I., Garrod, R. T., van Dishoeck, E. F., & Linnartz, H. 2009, A&A, 504, 891

Palumbo, M. E. 2006, A&A 453, 903

Palumbo, M. E., & Strazzulla, G. 1992, A&A, 259, L12

Palumbo, M. E., Baratta, G. A., Brucato, J. R., et al. 1998, A&A, 334, 247

Palumbo, M. E., Castorina, A. C., & Strazzulla, G. 1999, A&A, 342, 551

Palumbo, M. E., Ferini, G., & Baratta, G. A. 2004, Adv. Space Res., 33, 49

Palumbo, M. E., Baratta, G. A., Leto, G., & Strazzulla, G. 2010, J. Mol. Structure, 972, 64

Pedersen, A., & Gómez De Castro, A. I. 2011, ApJ, 740, 77

Prasad, S. S., & Tarafdar, S. P. 1983, ApJ, 267, 603

Roux, J. A., Wood, B. E., Smith, A. M., & Plyler, R. R. 1980, Arnold Engineering Development Center Final Report AEDC-TR-79-81 (Arnold Air Force Station)

Sandford, S. A., & Allamandola, L. J. 1990, ApJ, 355, 357

Sandford, S. A., Bernstein, M. P., Allamandola, L. J., Goorvitch, D., & Teixeira, T. C. V. S. 2001, ApJ, 548, 836

Shemansky, D. E., Matheson, P., Hall, D. T., Hu, H.-Y., & Tripp, T. M. 1993, Nature, 363, 329

Shen, C. J., Greenberg, J. M., Schutte, W. A., & van Dishoek, E. F. 2004, A&A, 415, 203

Sicilia, D., Ioppolo, S., Vindigni, T., Baratta, G. A., & Palumbo, M. E. 2012, A&A, 543, A155

Skinner, C. J., Tielens, A. G. G. M., Barlow, M. J., & Justtanont, K. 1992, ApJ, 399, L79

Smith, M. A. H., Rinsland, C. P., Fridovich, B., & Rao, K. N. 1985, in Molecular Spectroscopy: Modern Research, Vol. III, ed. K. N. Rao (Academic Press, London), 111

Strazzulla, G., & Johnson, R. E. 1991, in Comets in the post-Halley era, 1 (Dordrecht: ASSL Series), 243

Strazzulla, G., Pirronello, V., & Foti, G. 1983a, A&A, 123, 93

Strazzulla, G., Pirronello, V., & Foti, G. 1983b, ApJ, 271, 255

Strazzulla, G., Baratta, G. A., & Palumbo, M. E. 2001, Spectrochim. Acta A, 57, 825

Swordy, S. P. 2001, Space Sci. Rev., 99, 85

Westley, M. S., Baragiola, R. A., Johnson, R. E., & Baratta, G. A. 1995a, Nature, 373, 405

Westley, M. S., Baragiola, R. A., Johnson, R. E., & Baratta, G. A. 1995b, Planet Space Sci., 43, 1311

Wu, Y. J., Wu, C. Y. R., Chou, S. L., et al. 2012, ApJ, 746, 175

Ziegler, J. F., Ziegler, M. D., & Biersack, J. P. 2008, The stopping and range of ions in solids (New York: Pergamon Press), http://www.srim.org